Mineralogical Magazine, June 2016, Vol. 80(4), pp. 675–690

Lead-antimony sulfosalts from Tuscany (Italy). XVII. Meerschautite, $(Ag,Cu)_{5.5}Pb_{42.4}(Sb,As)_{45.1}S_{112}O_{0.8}$, a new expanded derivative of owyheeite from the Pollone mine, Valdicastello Carducci: occurrence and crystal structure

Cristian Biagioni[1,*], Yves Moëlo[2], Paolo Orlandi[1] and Chris J. Stanley[3]

[1] Dipartimento di Scienze della Terra, Università di Pisa, Via S. Maria 53, I-56126 Pisa, Italy
[2] Institut des Matériaux Jean Rouxel, UMR 6502, CNRS, Université de Nantes, 2, rue de la Houssinière, 44 322 Nantes Cedex 3, France
[3] Department of Earth Sciences, The Natural History Museum, Cromwell Road, London SW7 5BD, UK

[*Received 16 April 2015; Accepted 9 June 2015; Associate Editor: Peter Leverett*]

ABSTRACT

The new mineral species meerschautite, ideally $(Ag,Cu)_{5.5}Pb_{42.4}(Sb,As)_{45.1}S_{112}O_{0.8}$, has been discovered in the baryte + pyrite ± (Pb-Zn-Ag) deposit of the Pollone mine, near Valdicastello Carducci, Apuan Alps, Tuscany, Italy. It occurs as black prismatic crystals, striated along [100], up to 2 mm long and 0.5 mm thick, associated with baryte, boulangerite, pyrite, quartz and sphalerite. Meerschautite is opaque with a metallic lustre and shows a black streak. In reflected light, meerschautite is white in colour, weakly bireflectant and non pleochroic. With crossed polars, it is distinctly anisotropic with grey to dark grey rotation tints with brownish and greenish shades. Reflectance percentages for COM wavelengths [λ (nm), R_{air} (%)] are: 470: 39.7/41.4; 546: 38.3/39.9; 589: 37.4/39.0; 650: 35.8/37.2. Electron-microprobe data collected on two different samples gave (wt.%): Cu 0.22, Ag 3.15, Tl 0.07, Pb 48.54, Sb 25.41, As 2.82, S 19.74, Se 0.14, Cl 0.03, sum 100.12 (# 1) and Cu 0.22, Ag 3.04, Tl 0.13, Pb 48.53, Sb 25.40, As 2.93, Bi 0.06, S 19.82, Se 0.13, Cl 0.05, sum 100.31 (# 2). On the basis of 112 anions (S+Se+Cl) per formula unit, the empirical formulae are $(Ag_{5.29}Cu_{0.63})_{\Sigma 5.92}(Pb_{42.43}Tl_{0.06})_{\Sigma 42.49}(Sb_{37.80}As_{6.82})_{\Sigma 44.62}(S_{111.53}Se_{0.32}Cl_{0.15})_{\Sigma 112}$ (# 1) and $(Ag_{5.08}Cu_{0.62})_{\Sigma 5.70}(Pb_{42.22}Tl_{0.12})_{\Sigma 42.34}(Sb_{37.61}As_{7.07}Bi_{0.05})_{\Sigma 44.73}(S_{111.45}Se_{0.30}Cl_{0.25})_{\Sigma 112}$ (# 2). Main diffraction lines, corresponding to multiple *hkl* indices, are [*d* in Å (relative visual intensity)]: 3.762 (m), 3.663 (s), 3.334 (vs), 3.244 (s), 3.016 (m), 2.968 (m), 2.902 (m), 2.072 (ms). The crystal structure study gave a monoclinic unit cell, space group $P2_1$, with $a = 8.2393(1)$, $b = 43.6015(13)$, $c = 28.3688(8)$ Å, $\beta = 94.128(2)°$, $V = 10164.93(2)$ Å^3, $Z = 2$. The crystal structure has been solved and refined to a final $R_1 = 0.122$ on the basis of 49,037 observed reflections. The structure is based on two building blocks, both formed by a complex column with a pseudotrigonal Pb_6S_{12} core and two arms of unequal lengths (short and long arms, respectively). Two different kinds of short arms occur in meerschautite. One is an Ag-rich arm, whereas the other shows localized Sb–O–Sb bonds. Meerschautite is an expanded derivative of owyheeite and has quasi-homeotypic relationships with sterryite and parasterryite.

Keywords: meerschautite, new mineral species, sulfosalt, lead, silver, antimony, arsenic, oxygen, crystal structure, Pollone mine, Apuan Alps, Tuscany, Italy.

Introduction

The small baryte + pyrite ± (Pb-Zn-Ag) deposit exploited at the Pollone mine, near Valdicastello Carducci, has been known by the mineralogical community since the mid 1840s, when Kerndt

*E-mail: biagioni@dst.unipi.it
DOI: 10.1180/minmag.2016.080.011

(1845) described the crystals of the rare lead-antimony-arsenic sulfosalt geocronite. Since 2007, the scientific interest for this locality has been renewed by the discovery of a complex sulfosalt assemblage occurring in the micro-crystalline baryte + pyrite ore bodies. The mineralogical study of a large suite of samples allowed the identification of two new minerals, parasterryite and carducciite (Moëlo *et al*., 2011; Biagioni *et al*., 2014), as well as other sulfosalt species (sterryite, twinnite, chovanite, boulangerite and zinkenite).

Recently, some crystals having a monoclinic unit cell close to but distinct from those of sterryite and parasterryite were identified and characterized as a new mineral species, meerschautite. This name honours Alain Meerschaut (b. 1945), Research Director at the Centre national de la recherche scientifique (CNRS) (now retired), chemist-crystallographer in the field of solid-state chemistry at the Institut des Matériaux Jean Rouxel, Nantes, France, for his outstanding contribution to the definition and crystal structure study of new lead-antimony sulfosalts from Apuan Alps hydrothermal ores, i.e. scainiite, pillaite, pellouxite, rouxelite, moëloite and marrucciite. The mineral and its name have been approved by the IMA CNMNC (IMA 2013–061, Biagioni *et al*., 2013). The holotype specimen of meerschautite is deposited in the mineralogical collection of the Museo di Storia Naturale, Università di Pisa, via Roma 79, Calci (PI), Italy, with catalogue number 19649. Co-type specimens are deposited at the Musée de Minéralogie (MINES Paris Tech – old 'Ecole des Mines de Paris'), Paris, France, under catalogue number 83264 and at the Natural History Museum, London, UK, with catalogue number 2015,2.

This paper presents the definition and the crystal structure of meerschautite which appears, like sterryite and parasterryite, as a complex expanded derivative of owyheeite, $Ag_3Pb_{10}Sb_{11}S_{28}$.

Geological setting and occurrence

The Pollone mine (43°57′47″N; 10°16′19″E), near the small hamlet of Valdicastello Carducci, Pietrasanta, Tuscany, Italy, belongs to the group of baryte + pyrite ± iron oxides (magnetite and hematite) ore deposits exploited up to end of 1980s in the southern Apuan Alps. The two most important mines, i.e. the Pollone and the Monte Arsiccio mines, are located in the Sant'Anna tectonic window, an area in which metamorphic rocks belonging to the Apuan Alps metamorphic complex are surrounded by the non-metamorphic sedimentary formations of the Tuscan Nappe. In particular, the Pollone mine, located in the southern part of the tectonic window, exploited a baryte + pyrite ± (Pb-Zn-Ag) mineralization hosted within the Scisti di Fornovolasco Formation (Pandeli *et al*., 2004). This formation is composed of a Paleozoic – Early Triassic (?) metavolcanic–metasedimentary sequence, metamorphosed up to greenschist facies. Costagliola *et al*. (1998) recognized two kinds of orebodies, i.e. conformable lens-shaped ore bodies, mainly formed by microcrystalline baryte + pyrite, and baryte-quartz-pyrite-Pb-Zn-(Ag) vein systems. Estimates of *P-T* conditions indicate that host and country rocks record metamorphic temperatures of ~350°C, on the basis of chlorite and arsenopyrite geothermometers, with a pressure of 0.35 GPa, based on the phengite geobarometer (Costagliola *et al*., 1998). Appreciably higher temperatures (~450°C) were found for the mineralizing fluids.

Meerschautite has been identified in only a few samples collected in a microcrystalline baryte + pyrite ore body at the Pizzone stope, near the contact with the footwall schists. Crystals of meerschautite are scattered in the micro-crystalline baryte and only rarely protruded in small vugs. Associated minerals are baryte, boulangerite, pyrite, quartz and yellow crystals of sphalerite.

Mineral description

Physical and optical properties

Meerschautite occurs as lead-grey to black prismatic crystals, striated parallel to the elongation (**a** axis), up to 2 mm long and 0.5 mm wide (Fig. 1). It is brittle, with a perfect cleavage parallel to **a**; fracture is conchoidal. Streak is black and the lustre is metallic. Under the microscope, in polarized reflected light, meerschautite appears white in colour, without internal reflections. It is not pleochroic and it is weakly bireflectant. With crossed polars, it is distinctly anisotropic, with grey to dark grey rotation tints and brownish and greenish shades. The twinning, revealed by the X-ray study, could not be observed.

Reflectance has been measured in air on a section parallel to the elongation, with SiC as a standard; reflectance values are given in Table 1, whereas Fig. 2 shows the reflectance curves, compared with those of parasterryite (Moëlo *et al*., 2011). The Vickers hardness was not measured, owing to the small size and scarcity of the available crystals. Similarly, density was not measured, owing to the

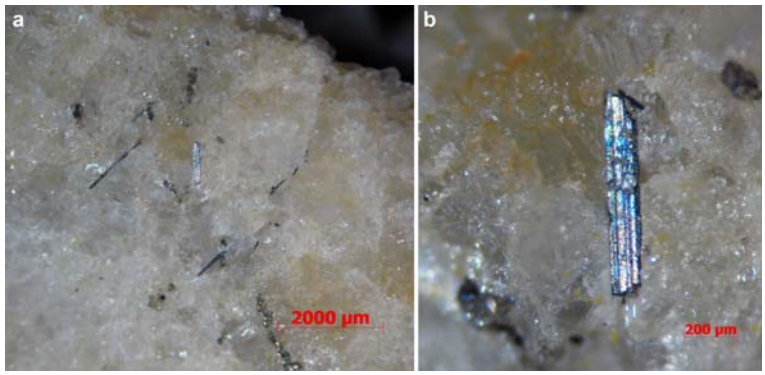

FIG. 1. Meerschautite, striated prismatic crystals embedded in microcrystalline baryte. Specimen # 19649, Museo di Storia Naturale, University of Pisa.

same reasons. Using the empirical formulae of samples 1 and 2 (see below), the calculated densities are 5.924 and 5.908 g·cm^{-3}, respectively.

Chemical analysis

Electron-microprobe analyses (WDS mode) were carried out with a CAMECA SX100 apparatus at 20 kV and 20 nA, with a 1 µm beam diameter. Only the following elements with $Z > 10$ were detected: Pb, Sb, S, Ag, Cu, Tl, Bi, Se and Cl. Standards (element, emission line, counting time) are: PbS (Pb*M*α, 30 s), stibnite (Sb*L*α, 30 s), pyrite (S*K*α, 50 s), Ag metal (Ag*L*α, 30 s), AsGa (As*L*α, 40 s), Cu metal (Cu*K*α, 30 s), lorándite (Tl*M*α, 20 s), Bi metal (Bi*M*α, 20 s), Se metal (Se*L*α, 40 s) and pyromorphite (Cl*K*α, 40 s). Cadmium, indium and mercury were sought but were found below the detection limit (0.15, 0.06 and 0.08 wt.%, respectively). The O content, revealed by the crystal-structure study (see below), was too low (~0.09 wt.%) to be detected by electron-microprobe analysis (Orlandi *et al.*, 2001; Orlandi *et al.*, 2004). Analytical results are given in Table 2.

On the basis of 112 (S+Se+Cl) atoms per formula unit (apfu), the empirical formulae for the two analysed grains (samples 1 and 2) are as follows:

$$(Ag_{5.29}Cu_{0.63})_{\Sigma 5.92}(Pb_{42.43}Tl_{0.06})_{\Sigma 42.49}$$
$$(Sb_{37.80}As_{6.82})_{\Sigma 44.62}(S_{111.53}Se_{0.32}Cl_{0.15})_{\Sigma 112} \quad (1)$$

$$(Ag_{5.08}Cu_{0.62})_{\Sigma 5.70}(Pb_{42.22}Tl_{0.12})_{\Sigma 42.34}$$
$$(Sb_{37.61}As_{7.07}Bi_{0.05})_{\Sigma 44.73}(S_{111.45}Se_{0.30}Cl_{0.25})_{\Sigma 112} \quad (2)$$

Applying the substitutions $Tl^{+} + Sb^{3+} = 2\ Pb^{2+}$, $Ag^{+} + Bi^{3+} = 2\ Pb^{2+}$ and $Pb^{2+} + Cl^{-} = Sb^{3+} + S^{2-}$, the following formulae can be obtained:

$$(Ag_{5.29}Cu_{0.63})_{\Sigma 5.92}Pb_{42.40}$$
$$(Sb_{37.89}As_{6.82})_{\Sigma 44.71}(S_{111.68}Se_{0.32})_{\Sigma 112} \quad (1)$$

$$(Ag_{5.03}Cu_{0.62})_{\Sigma 5.65}Pb_{42.31}$$
$$(Sb_{37.74}As_{7.04})_{\Sigma 44.78}(S_{111.70}Se_{0.30})_{\Sigma 112}. \quad (2)$$

The valence equilibrium *Ev*, defined as $Ev\ (\%) = [\Sigma(\text{val}+) - \Sigma(\text{val}-)] \times 100/\Sigma(\text{val}-)$, is +0.38 and +0.27 for formulae (1) and (2), respectively. These formulae can be simplified as $(Ag,Cu)_6Pb_{42.3}(Sb,As)_{44.7}S_{112}$, which is very close to charge balance, with the excess of about one positive charge, not

TABLE 1. Reflectance data for meerschautite in air.

λ/nm	R_{min}	R_{max}	λ/nm	R_{min}	R_{max}
400	41.1	43.1	560	38.0	39.6
420	40.6	42.4	580	37.6	39.2
440	40.1	41.8	**589**	**37.4**	**39.0**
460	39.8	41.5	600	37.1	38.7
470	**39.7**	**41.4**	620	36.6	38.1
480	39.5	41.2	640	36.0	37.5
500	39.2	40.8	**650**	**35.8**	**37.2**
520	38.8	40.5	660	35.5	36.9
540	38.5	40.0	680	35.0	36.4
546	**38.3**	**39.9**	700	34.6	36.0

The reference wavelengths required by the Commission on Ore Mineralogy (COM) are given in bold.

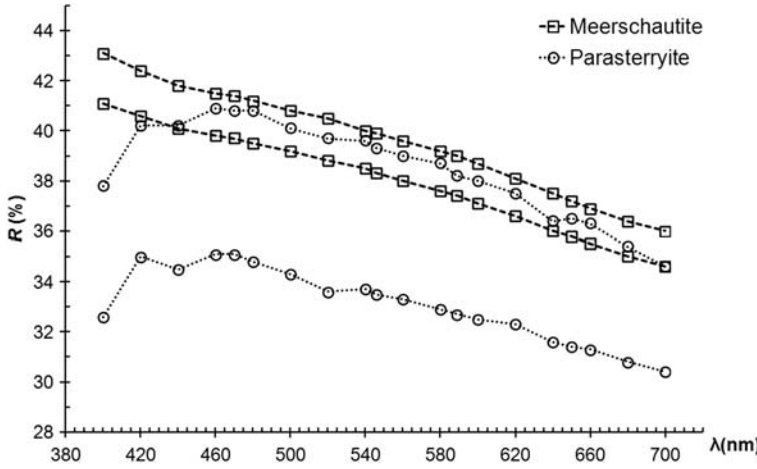

FIG. 2. Reflectance spectrum of meerschautite. For comparison, the reflectance spectrum of parasterryite in air is also shown (Moëlo *et al*., 2011).

taking into account the small oxygen content revealed by the structural study (see below).

Crystallography

The powder X-ray diffraction pattern of meerschautite was obtained using a 114.6 mm diameter Gandolfi camera, with Ni-filtered Cu*K*α radiation. The observed powder X-ray diffraction pattern is compared in Table 3 with that calculated using the software *PowderCell* 2.3 (Kraus and Nolze, 1996). Unit-cell parameters were not refined from the powder X-ray diffraction data because of the multiplicity of indices for the majority of diffraction lines.

For the single-crystal X-ray study, the intensity data were collected using a Bruker Smart Breeze diffractometer equipped with an air-cooled CCD detector, with graphite-monochromatized Mo*K*α radiation. The detector-to-crystal distance was 50 mm. A total of 1179 frames were collected using ω and φ scan modes, in 0.3° slices, with an exposure time of 45 s per frame. The data were corrected for the Lorentz, polarization, absorption and background effects using the software package *Apex*2 (Bruker AXS Inc., 2004).

TABLE 2. Microprobe analyses of meerschautite: chemical composition as wt.%.

	sample 1			sample 2		
Element	wt.%	Range (n = 3)	e.s.d.	wt.%	Range (n = 3)	e.s.d.
Cu	0.22	0.21–0.24	0.02	0.22	0.20–0.24	0.02
Ag	3.15	3.05–3.25	0.10	3.04	3.00–3.10	0.05
Tl	0.07	0.05–0.09	0.02	0.13	0.12–0.13	0.01
Pb	48.54	48.42–48.74	0.18	48.53	48.04–48.89	0.44
Sb	25.41	25.35–25.51	0.09	25.40	25.20–25.58	0.19
As	2.82	2.80–2.85	0.03	2.93	2.92–2.94	0.01
Bi	n.d.	–	–	0.06	0.02–0.09	0.04
S	19.74	19.69–19.79	0.05	19.82	19.79–19.86	0.04
Se	0.14	0.04–0.21	0.09	0.13	0.11–0.16	0.03
Cl	0.03	0.03–0.04	0.01	0.05	0.04–0.05	0.01
sum	100.12	100.05–100.24	0.10	100.31	99.57–100.76	0.64

TABLE 3. Powder X-ray diffraction data for meerschautite.

d_{obs}	I_{obs}	d_{calc}	I_{calc}	$h\ k\ l$	d_{obs}	I_{obs}	d_{calc}	I_{calc}	$h\ k\ l$
		7.13	12	0 4 3			2.967	53	0 8 8
4.25	mw	4.31	4	0 10 1	**2.968**	**m**	2.958	14	2 10 1
4.16	w	4.15	31	0 5 6			2.957	12	$\bar{2}$ 10 2
		3.974	10	0 2 7			2.941	12	2 6 5
		3.958	5	0 10 3			2.926	12	2 9 3
3.959	mw	3.956	8	0 6 6			2.925	15	$\bar{2}$ 9 4
		3.954	5	2 3 0			2.895	35	2 10 2
		3.954	5	$\bar{2}$ 3 1	**2.902**	**m**	2.894	39	$\bar{2}$ 10 3
3.927	w	3.925	27	0 11 1			2.891	12	0 15 1
3.840	vw	3.844	10	$\bar{2}$ 4 1			2.886	12	2 4 6
3.762	**m**	3.760	51	0 7 6			2.858	16	2 7 5
3.663	**s**	3.667	96	0 5 7			2.857	17	$\bar{2}$ 7 6
3.601	mw	3.604	26	0 12 1	2.823	w	2.824	15	2 11 1
		3.566	19	0 8 6			2.824	14	$\bar{2}$ 11 2
3.555	vw	3.560	26	2 3 3			2.808	10	2 10 3
		3.558	29	$\bar{2}$ 3 4			2.808	16	$\bar{2}$ 10 4
3.516	vw	3.519	2	0 12 2			2.770	18	2 11 2
		3.479	27	2 4 3	2.773	m	2.769	19	$\bar{2}$ 11 3
3.454	vw	3.478	23	$\bar{2}$ 4 4			2.766	14	$\bar{2}$ 6 7
		3.437	16	0 3 8	2.722	mw	2.723	14	0 8 9
3.359	w	3.354	6	2 3 4			2.698	8	2 7 6
		3.352	6	$\bar{2}$ 3 5	2.698	mw	2.697	9	2 4 7
3.393	vw	3.384	14	2 5 3			2.696	8	$\bar{2}$ 7 7
3.334	**vs**	3.331	100	0 13 1			2.695	7	$\bar{2}$ 4 8
		3.286	13	2 4 4	2.635	vw	2.637	3	0 9 9
		3.285	21	$\bar{2}$ 4 5	2.605	vw	2.601	3	2 11 4
		3.278	25	0 5 8	2.553	w			
3.244	**s**	3.247	79	0 8 7	2.462	vw	2.463	4	$\bar{2}$ 14 2
3.218	w	3.206	16	2 5 4	2.408	w	2.400	8	2 2 9
		3.204	13	$\bar{2}$ 5 5			2.398	7	$\bar{2}$ 2 10
3.116	w	3.114	7	0 14 0	2.375	vw	2.382	8	2 3 9
		3.114	6	2 6 4			2.380	8	$\bar{2}$ 3 10
3.095	w	3.096	14	0 14 1	2.349	vw	2.354	5	0 1 12
		3.076	11	0 7 8	2.281	vw	2.283	3	$\bar{2}$ 9 9
		3.045	11	2 8 3	2.251	mw	2.244	11	2 2 10
		3.025	21	2 9 2			2.242	15	$\bar{2}$ 2 11
		3.024	14	$\bar{2}$ 9 3	2.165	m	2.159	14	0 16 8
3.016	**m**	3.016	12	2 7 4	2.109	vw	2.109	5	$\bar{2}$ 1 12
		2.990	11	2 10 0	**2.072**	**ms**	2.076	13	0 17 8
		2.990	15	$\bar{2}$ 10 1			2.060	90	$\bar{4}$ 0 1
					2.030	m	2.034	11	0 20 5
					2.005	mw	2.002	11	0 3 14

The eight strongest reflections are given in bold.
Intensities and d_{hkl} values were calculated using the software *PowderCell 2.3* (Kraus and Nolze, 1996) on the basis of the structural model. Observed intensities were visually estimated. vs = very strong; s = strong; ms = medium-strong; m = medium; mw = medium-weak; w = weak; vw = very weak. Only reflections with $I_{calc} > 5$ are listed, if not observed.

The statistical tests on the distribution of $|E|$ values ($|E^2-1| = 0.750$) and the systematic absences suggested the acentric space group $P2_1$. The refined unit-cell parameters are a = 8.2393(1), b = 43.6015(13), c = 28.3688(8) Å, β = 94.128(2), V = 10,164.93(2) Å^3. The a:b:c ratio is 0.189:1:0.651. The crystal structure was solved and refined using *Shelx*-97 (Sheldrick, 2008). Scattering curves for neutral atoms were taken from the *International Tables for Crystallography* (Wilson,

TABLE 4. Crystal data and summary of parameters describing data collection and refinement for meerschautite.

Crystal data	
X-ray formula	$(Ag_{5.05}Cu_{0.50})_{\Sigma 5.55}Pb_{42.33}(Sb_{38.37}As_{6.75})_{\Sigma 45.12}S_{112}O$
Crystal size (mm^3)	0.090 × 0.009 × 0.006
Cell setting, space group	Monoclinic, $P2_1$
a, b, c (Å); α, β, γ (°)	8.2393(1), 43.6015(13), 28.3688(8); 90.00, 94.128(2), 90.00
V (Å^3)	10,164.93(2)
Z	2
Data collection and refinement	
Radiation, wavelength (Å)	Mo$K\alpha$, λ = 0.71073
Temperature (K)	293
Maximum observed 2θ (°)	65.37
Measured reflections	131,019
Unique reflections	64,972
Reflections $F_o > 4\sigma(F_o)$	49,037
R_{int} after absorption correction	0.0605
$R\sigma$	0.1032
Range of h, k, l	$-12 \le h \le 12$, $-62 \le k \le 66$, $-42 \le l \le 38$
R [$F_o > 4\ \sigma\ F_o$]	0.1216
R (all data)	0.1546
wR (on)	0.2948
Goof	1.114
Number of least-squares parameters	1337
Maximum and minum residual peak (e/Å^3)	10.60; –18.70

1992). After having located the heavier atoms (Pb and Sb atoms), the lighter ones were found through successive difference-Fourier syntheses.

The crystal structure solution points out the existence of an atom layering according to the $(\bar{4}01)$ plane, with the [104] direction at an angle of 89.964° to the **a** axis. Consequently, a twinning with (001) as twin plane is possible, as observed in sterryite and parasterryite. The introduction of such a twinning improved the refinement; the twin ratio is 0.29(1):0.71(1). As observed in sterryite and parasterryite, as well as in other lead sulfosalts having a complex crystal chemistry, sites with mixed cation occupancies were found. Some of these sites could also be split in two sub-positions. The bond-valence method was applied to adjust the site occupancies as far as possible (Moëlo *et al*., 2012). The coordination of two Sb sites suggested the presence of an additional oxygen anion, giving rise to a configuration similar to those reported in other oxysulfosalts, e.g. scainiite (Moëlo *et al*., 2000). In addition, some split Sb or mixed (Pb/Sb) sites resulted from the necessity to avoid too short *Me–Me* distances. The site occupancies of such split positions were initially refined, pointing to a 50:50 occupancy; consequently, their site occupancy factors (s.o.f.) were fixed to this ratio.

The refinement converged to R_1 = 0.122 for 49,037 reflections with $F_o > 4\sigma(F_o)$ and 0.155 for all 64,972 reflections. Crystal data and details of the intensity data collection and refinement are reported in Table 4. The high maximum and minimum peak residuals could be related to the low diffraction quality of the available crystals, characterized by twinning and, as hypothesized by Moëlo *et al*. (2012) for sterryite and parasterryite, by order-disorder phenomena.

The structural formula of meerschautite is $(Ag_{5.05}Cu_{0.50})_{\Sigma 5.55}Pb_{42.33}(Sb_{38.37}As_{6.75})_{\Sigma 45.12}S_{112}O$, with an *Ev* value of –0.19%. The crystallographic information file, containing atom positions, displacement parameters and bond distances has been deposited with the Principal Editor of Mineralogical Magazine and is available from www.minersoc.org/pages/e_journals/dep_mat_mm.html

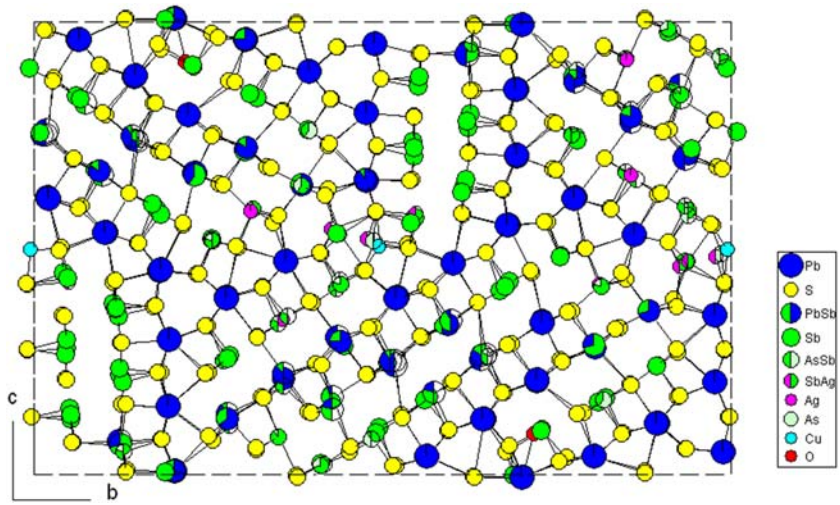

FIG. 3. Projection along **a** of the crystal structure of meerschautite. The longest (Sb,As)–S bonds have been omitted for clarity.

Crystal-structure description

General organization of meerschautite

The unit-cell content of meerschautite, as seen down **a** is presented in Fig. 3. The structure of meerschautite is based on two building blocks, both formed by a complex column with a pseudotrigonal Pb_6S_{12} core and two 'arms' of unequal lengths (Fig. 4). The structure of meerschautite is topologically very similar to those of sterryite and parasterryite (Moëlo *et al*., 2012) and differs in the configuration and composition of the shorter arms. In meerschautite, two different kinds of short arms occur, connecting successive pseudotrigonal columns along **c**: one is a (Pb,Sb) arm characterized by the occurrence of localized Sb–O–Sb bonds (column A), whereas the other is an Ag-rich arm (column B). The first arm has composition $Pb_{2.30}(Sb_{3.00}As_{0.70})_{\Sigma 3.70}S_8O$ (= Me_6S_8O), whereas the second one has chemical formula $Cu_{0.50}Ag_2(Sb_{3.15}As_{1.35})_{\Sigma 4.50}S_8$ (= Me_7S_8). These two types of arms can be compared with those occurring in sterryite and parasterryite, $CuSb_2Pb(Pb,Sb)(As–As)S_8$ and $Ag_2(Pb,As)Sb(Sb,As)As_3S_{10}$ (Moëlo *et al*., 2011, 2012), respectively.

The halved unit formula of meerschautite contains $Me_{46.5}S_{56}O_{0.5}$, half a cation in defect with respect to sterryite ($Me_{47}S_{56}$) and 1.5 *Me* and 2 S atoms less than parasterryite ($Me_{48}S_{58}$). Comparing the atom topology of the two types of columns (Fig. 5) occurring in meerschautite with those reported in sterryite and parasterryite, without distinction of cation species, they have in common the prismatic core and the long arm, as well as a Me_2S_4 group at the base of the short arm, i.e. a $Me_{42}S_{52}$ atom group (total 94 atoms). Actually, in the (Pb,Sb) arm, the group at the base of the arm is $(Sb_{1.00}Pb_{0.80}As_{0.20})S_4$, whereas in the Ag-rich arm, the group at its base is $(Sb_{1.5}Ag_{0.5})_{\Sigma 2}S_4$. Non-equivalent atom positions in the short arms correspond to $Pb(Pb_{0.50}Sb_{0.50})Sb_2S_4O$ in the (Pb, Sb) arm (nine atoms) and $(Cu_{0.50}As_{0.50})Ag(Ag_{0.50}Sb_{0.50})(As_{0.65}Sb_{0.35})(Sb_{0.80}As_{0.20})S_4$ in the Ag-rich arm (nine atoms). Taking into account the non-equivalent atom positions in the short arms of meerschautite, the similarity index (i.e. the percentage of atom positions with equivalent topology – Orlandi *et al*., 2007) between the two constituting complex columns in meerschautite, that is the ratio (common positions)/(total atoms of the formula unit), is 94/103 for both columns A and B. Consequently, the similarity index between the two complex modules is ~91.3%.

As described above, the crystal structure shows layers of atoms parallel to the $(\bar{4}01)$ plane (Fig. 6); such a layered atom distribution suggests the possible occurrence of a (pseudo)-orthorhombic superstructure, with unit-cell parameters $a' = a$, $b' = b$, $c' = 113.2$ Å, $\beta = 90.0(8)°$, $V' = 4V = 40{,}659$ Å^3, $Z = 8$. Unfortunately, superstructure reflections were not observed during data collection. Meerschautite is one of the lead sulfosalts with the largest unit-cell volume, i.e. ~10,165 Å^3, to be compared with those of tazieffite (10,257 Å^3),

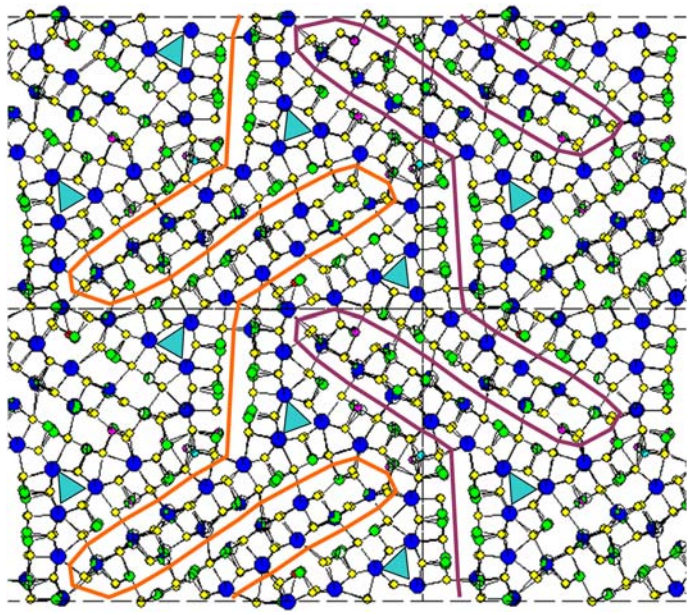

FIG. 4. Enlarged projection along **a** of the crystal structure of meerschautite. Orange (at left) and violet (at right) lines limit along **c** one zig-zag layer of fundamental building blocks, i.e. complex columns organized around a triangular prismatic core. Symbols as in Fig. 3.

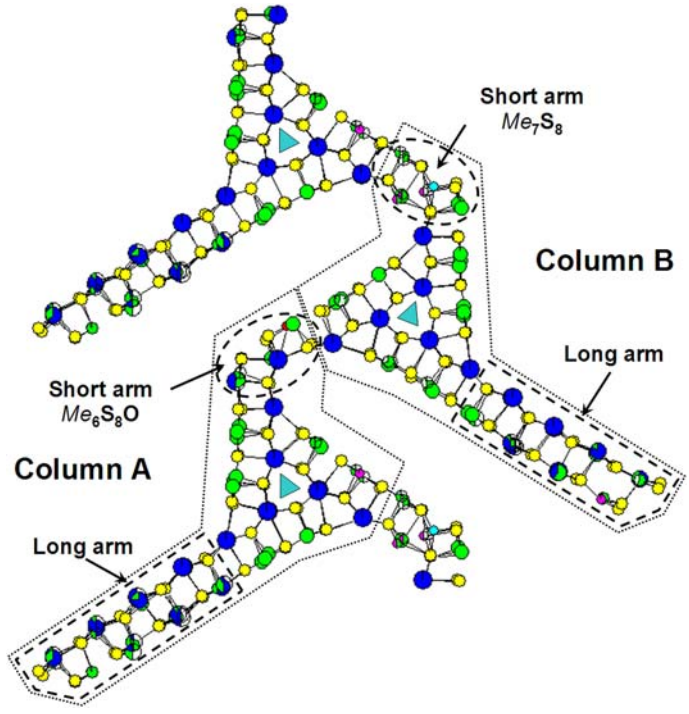

FIG. 5. Details of the two complex columns representing the fundamental building blocks in meerschautite.

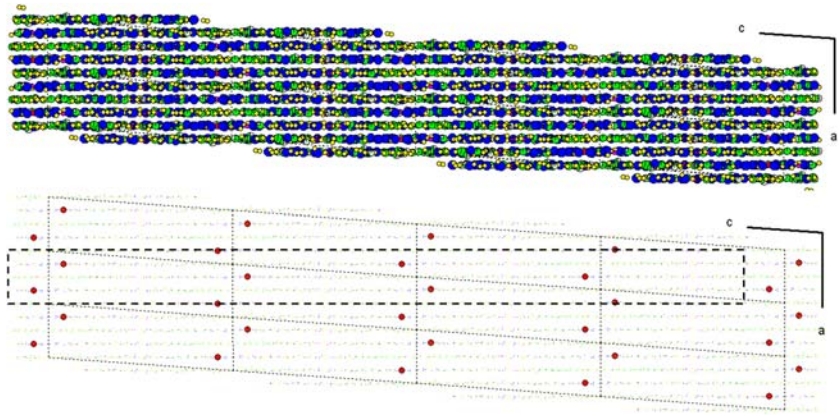

FIG. 6. Projection along **b** of the crystal structure of meerschautite, showing the atom layering. The hypothetical orthorhombic super-cell is shown below [only oxygen atoms (red circles) are represented].

vurroite (10,265 Å^3) and parasterryite (10,300 Å^3). Actually, the unit-cell volumes of vurroite (Pinto *et al*., 2008) and, possibly, tazieffite (Zelenski *et al*., 2009) correspond to those of the sub-structures, with doubling of the *c* parameter in the real structures.

Columns organization, cation coordination, and site occupancies

Two symmetry-independent complex columns, i.e. column A and column B, occur in the crystal structure of meerschautite. As described briefly above, they are organized around a triangular prismatic core, with a long arm and a short arm (Fig. 5). In the description of the two complex columns, the coordination polyhedra of the several Pb, Sb and As positions will not be detailed, owing to the complexity of the structure and the relatively poor *R* value. The Pb coordination number ranges between VI and IX, corresponding to octahedral, mono-, bi- and tricapped triangular prismatic coordinations. The Sb, (Sb/As) and As sites usually show an asymmetric coordination, due to the strong activity of the lone electron pair; the unsplit sites generally have three bond distances shorter than 2.70 Å, whereas split ones show different coordinations, having in some cases only two distances shorter than 2.70 Å but three or four bond distances shorter than 3 Å. The coordination of Ag and Cu atoms will be discussed below, whereas minor Tl and Bi have not been localized directly in the crystal structure of meerschautite. As in sterryite, thallium and bismuth may be hosted at the largest and smallest Pb sites in the crystal structure of meerschautite.

According to the crystal structure refinement, column A has composition $Ag_{2.05}Pb_{22.43}(Sb_{19.27}As_{2.25})_{\Sigma 21.52}S_{56}O$, containing 16 pure Pb sites, nine pure Sb sites (four of them are split) and two pure Ag sites. In addition, 13 [Pb/(Sb,As)], five (Sb/As) and one (Sb/Ag) positions, in some cases as split sites, occur; in only one (Sb/As) site, As > Sb. The pure Ag sites occur at the end of the long arm, on the *C*2 face and on the *A* face [see fig. 6 in Moëlo *et al*. (2012) for faces notation]. Regarding the former, the Ag25A site alternates with a mixed (Sb, As) site (Sb26A), in the same configuration reported in the crystal structures of sterryite and parasterryite (Moëlo *et al*., 2012). This Ag atom has a strongly distorted octahedral coordination, with four relatively short bond distances (ranging between 2.64 and 2.82 Å) and two longer ones (3.04 and 3.12 Å). The Ag11A occurs on the *A* face, and was interpreted initially as an average position of an Sb atom. However, its bond-valence sum (BVS) was very low (1.84 valence units, vu), with only one bond distance shorter than 2.70 Å; consequently, an Ag-site occupancy with a three-fold coordination (taking into account bond distances shorter than 3 Å) was hypothesized, achieving a BVS of 0.82 vu. This Ag atom has a distorted square pyramidal coordination, with two linear bonds at 2.76 and 2.94 Å and a third bond at 2.45 Å (the angle S08A–Ag11A–S15A being ~93°). The coordination sphere is completed by two additional longer bonds both at 3.22 Å.

An interesting feature displayed by the column A is the localized Sb–O–Sb bonds at the end of the

short arm. The occurrence of this kind of bond was hypothesized because the Sb45A and Sb46A atoms have only two Sb–S distances shorter than 2.70 Å, as observed in other oxysulfosalts (e.g. scainiite, Moëlo *et al*., 2000). Whereas Sb46A has a pure Sb site occupancy, the bond distances and the refined site scattering suggest a mixed (Sb,As) occupancy at the Sb45A position. The BVS at the Sb45A and Sb46A are 3.31 and 2.90 vu, respectively. The BVS have been calculated by using the bond parameters given by Brese and O'Keeffe (1991) for Sb–S, As–S and As^{3+}–O bonds, and by Mills *et al*. (2009) for the Sb^{3+}–O bond. The oxygen coordination is completed by a bond with Pb44A, at 2.82 Å; the total BVS of the oxygen atom is 1.81 vu. The site occupancy at the O site was fixed to 1, even if one cannot exclude a lower site occupancy, as suggested by the chemical analyses (s.o.f. ≈ 0.5) and the structural formula, that would be charge balanced with an O s.o.f. of ~0.8. The possible existence of vacancy at the O site will be briefly discussed in a later section (see 'Crystal-chemistry of meerschautite').

The crystal structure refinement gives a chemical composition for column B as $Cu_{0.50}Ag_3Pb_{20.15}(Sb_{19}As_{4.35})_{\Sigma 23.35}S_{56}$, this column being richer in Ag and As than column A. It contains 15 pure Pb sites, nine pure Sb sites (three of them are split), and several mixed (Sb/As) and (Pb/Sb) sites, sometimes split. In addition, five Ag sites (four of them being only half-occupied) and one half-occupied Cu site occur. The Ag sites are concentrated at the end of the long arm, on the *C*2 face, as occurs in column A, and in the short arm. Ag26B alternates with a mixed (Sb,As) site, namely Sb25B, in the same configuration observed in column A and in the related minerals sterryite and parasterryite (Moëlo *et al*., 2012). This Ag atom has a distorted octahedral coordination, with bond distances ranging from 2.41 to 3.38 Å. The Ag-rich nature of column B is related to the occurrence of four half-occupied Ag sites in the short arm, namely Ag42B′, Ag44B, Ag45B and Ag46B′. Sites Ag42B′ and Ag46B′ are split positions of mixed (Ag,Sb) sites; the splitting is required in order to avoid too short *Me–Me* distances. A hypothetical ordered sequence of Ag sites along **a** of the short arm of complex column B is proposed in Fig. 7; notwithstanding such splits, it is not possible to avoid a short Ag–Ag distance (Ag44B–Ag46B′ = 2.90 Å). This distance can be compared with short Ag–Ag distances reported for other Ag sulfosalts, e.g. fettelite (2.75 Å – Bindi *et al*., 2009), debattistiite (2.83 and 2.76 Å – Guastoni *et al*., 2012), face-centred cubic

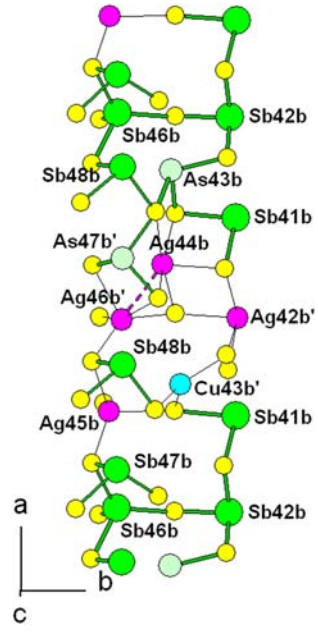

FIG. 7. Hypothetical ordered sequence of split sites within the short arm of column B in meerschautite.

silver (2.89 Å – Suh *et al*., 1988) and hexagonal close packed allargentum (2.92 Å – Petruk *et al*., 1970). In the Ag-rich arm of parasterryite, the Ag–Ag distance is 3.004 Å (Moëlo *et al*., 2012). The Ag sites have various geometries, from distorted octahedral, with bond distances ranging from 2.54 to 3.31 Å, to a five-fold hemi-octahedral.

In the crystal structure of sterryite, Cu preferentially occurs in a partially occupied site in the short arm, having a quasi-triangular coordination, with three bonds ranging from 2.28 and 2.29 Å, and a fourth one at 2.61 Å. On the contrary, in the crystal structure of meerschautite, the position of this cation, with a low content (0.6 apfu from electron-microprobe data), was sought among possible empty S tetrahedral sites but without success. Then, it was assumed that Cu is hosted at the split triangular site located in the short arm, with bond distances ranging between 2.23 and 2.37 Å. The next-nearest S neighbours is at 3.67 Å. The total BVS at the Cu site is 0.95 vu. Such a triangular coordination is not usual in lead-antimony sulfosalts; on the contrary it has been reported in some lead-bismuth sulfosalt, i.e. cuproneyite, $Cu_7Pb_{27}Bi_{25}S_{68}$ (Ilinca *et al*., 2012), eclarite, $Cu_{1.5}Pb_{7.75}Bi_{13}S_{28}$ (Topa and Makovicky, 2012), paděraite, $Cu_7(X_{0.33}Pb_{1.33}Bi_{11.33})_{\Sigma 13}S_{22}$, with X = Cu or Ag

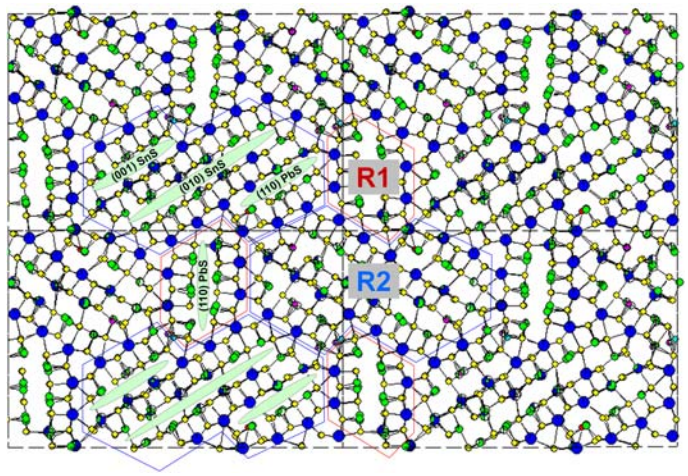

FIG. 8. Projection along **a** of the crystal structure of meerschautite, showing the two kinds of rods (A and B). Green ellipses: Me^{3+} lone electron-pair micelles.

(Topa and Makovicky, 2006) and pizgrischite, (Cu,Fe)$Cu_{14}PbBi_{17}S_{35}$ (Meisser *et al*., 2007).

Modular analysis

The crystal structure of meerschautite can be described according to a modular analysis in two ways (Moëlo *et al*., 2000), either on the basis of the organization around pseudo-ternary axes, or on the basis of Me^{3+} (*Me* = Sb, As) lone electron-pair micelles.

In the first approach, used above for the description of the structure, the complex columns characterizing meerschautite have been defined principally taking into account the surfaces of weakest bonding, cutting the longest (Sb,As)–S bonds along three distinct lone electron-pair micelles, in agreement with Moëlo *et al.* (2012). Each column is connected along **c** to two columns by their short arms to form a 'fish-bone' zigzag layer parallel to (010). The whole structure is generated by the interlocking of these layers along **b**. The pseudo-ternary cyclic rods constituting the core of the complex columns are typical of the phases belonging to the zinkenite group (Makovicky, 1985) and are topologically identical with the cyclic unit rods constituting the building blocks of hexagonal $Ba_{12}Bi_{24}S_{48}$ (Aurivillius, 1983).

Such an organization based on surfaces of weakest bonding indicates that the perfect cleavage observed parallel to **a** would correspond to the (010) plane.

In the second approach, the crystal structure can be cut into 1D building blocks (Fig. 8) directly derived from the SnS archetype (Makovicky, 1993): two types of rods (R1 and R2) can be defined. Within these two rods, the Me^{3+} lone electron pairs are organized to form infinite ribbon-like micelles along **a**. The simplest rod R1 is four-atoms thick, and three-octahedra large. This rod is similar to the constitutive $Pb_4Sb_6S_{14}$ rod of jamesonite (Léone *et al*., 2003). The marginal Fe atom connecting two rods in jamesonite is replaced here by cations of the two short arms [(Ag,Sb) or (Pb,Sb)]. The complex rod R2 is eight-atoms thick, and six-octahedra large; it is related structurally to the sartorite series, as indicated by Moëlo *et al.* (2012). The rods R1 and R2 present a small dissymmetry, as they have in common cations of the two short arms: Pb44A (bound to O) on one side, and the four Ag sites of the other arm at the other side.

The As/Sb partitioning has been enhanced in Fig. 9. The rod R1 is depleted in As (only one site with 0.2 As), while all As-rich sites are distributed at the periphery of R2. Indeed, the $As/(Sb+As)_{at.}$ is 0.105 and 0.186 for R1 and R2, respectively. Such a partitioning is in agreement with the Sb-rich structure type of R1, i.e. jamesonite, on the one hand, and, on the other hand, the As-rich structure type of R2, i.e. sartorite.

As indicated in Fig. 8, the two mono-atomic layers separated by the ribbon-like micelles are connected in three ways, according to $(110)_{PbS}$ and $(001)_{SnS}$ or $(010)_{SnS}$. Such an interface

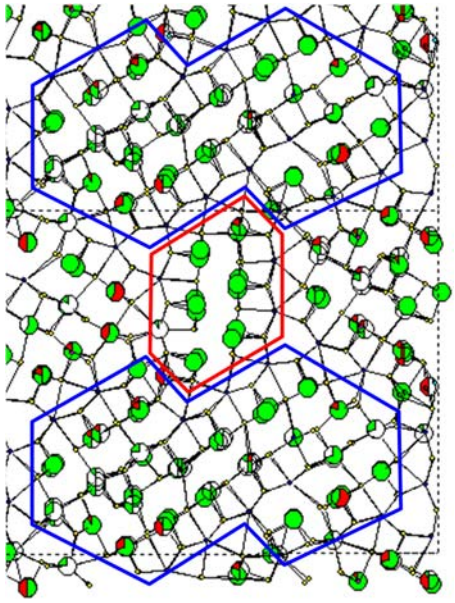

FIG. 9. As/Sb partitioning between R1 and R2 rods: As (red) and Sb (green) have been enhanced.

organization is distinct from those observed for sterryite and parasterryite (Moëlo *et al*., 2012).

Discussion

Crystal-chemistry of meerschautite

The crystal structure of meerschautite is very complex and a derivation of its simplified formula is not straightforward. The crystal structure study points to the presence of 93 cation sites, agreeing with the cation sums of chemical formulae (1) and (2), i.e. 93.03 and 92.74 apfu, respectively.

The chemical analyses suggest an idealized chemical formula $(Ag,Cu)_6Pb_{42.3}(Sb,As)_{44.7}S_{112}$, requiring only 0.35 O apfu for charge balance. Taking into account the oxygen content, the simplified formula $(Ag,Cu)_6Pb_{43-2x}(Sb,As)_{44+2x}S_{112}O_x$, with $x = 0.35$, could be proposed. The X-ray formula, $(Ag_{5.05}Cu_{0.50})_{\Sigma 5.55}Pb_{42.33}(Sb_{38.37}As_{6.75})_{\Sigma 45.12}S_{112}O$, pointed out two main differences with respect to this simplified formula: (1) the (Ag+Cu) content is a little bit lower, i.e. 5.5 apfu instead of 6 apfu; and (2) the x value should be closer to 1, and possibly equal to ~0.8, in order to achieve the electrostatic neutrality. Starting from the proposed simplified formula, if $x = 0.8$, then the formula of meerschautite should be $(Ag,Cu)_6Pb_{41.4}(Sb,As)_{45.6}S_{112}O_{0.8}$. Subtracting 0.5 Ag from this latter formula according to the substitution $Ag^+ + (Sb,As)^{3+} = 2\ Pb^{2+}$, the formula becomes $(Ag,Cu)_{5.5}Pb_{42.4}(Sb,As)_{45.1}S_{112}O_{0.8}$, in agreement with the X-ray formula.

The discrepancy between the oxygen content calculated from the chemical analysis and that revealed by the crystal structure refinement could derive from uncertainties in the chemical analysis (e.g. a slight overestimation of the Ag content) or from chemical inhomogeneities between different grains (or within the same grain), with two possible substitution mechanisms operating, (i) $2\ Pb^{2+} + \square = 2\ (Sb,As)^{3+} + O^{2-}$ and (ii) $Ag^+ + (Sb,As)^{3+} = 2\ Pb^{2+}$, or a combination of the two substitutions. It should be noted that the absence of oxygen coordinating the (Sb,As) atoms hosted at the Sb45A and Sb46A sites would require a shift of these atom positions in order to achieve a reasonable three-fold coordination with S atoms. Indeed, there are some hints indicating their possible splitting, in particular for the Sb46A, but unfortunately the quality of the diffraction data, as well as the probably low amount of vacancy at the

TABLE 5. Mineral species related to meerschautite.

Mineral	*a* (Å)	*b* (Å)	*c* (Å)	β (°)	*V* (Å^3)	S.G.
Owyheeite[1]	4.10	27.31	22.94	90.36	2571	$P2_1/c$
Sterryite Madoc[2]	28.4	42.6	8.26	90	9921	*Pba*2 *or Pbam*
Sterryite Pollone[3]	8.19	28.53	42.98	94.90	10,005	$P2_1/n$
Parasterryite[3]	8.40	27.95	43.88	90.06	10,300	$P2_1/c$
Tubulite[4]	4.13 (x 2)	43.1	27.4	93.2	4872 (x 2)	*P*2/*c*, *Pc* or $P2_1/c$
Meerschautite[5]	8.24	43.60	28.37	94.13	10,165	$P2_1$

[1]Laufek *et al*. (2007); [2]Jambor (1967); [3]Moëlo *et al*. (2011); [4]Moëlo *et al*. (2013); [5]this work.

TABLE 6. The sterryite plesiotypic series: structural formulae.

		Specific short arm
Sterryite	$Cu(Ag,Cu)_3Pb_{19}(Sb,As)_{22}(As\text{-}As)S_{56}$	$CuSb_2Pb(Pb,Sb)(As–As)S_8$
Parasterryite	$Ag_4Pb_{20}(Sb,As)_{24}S_{58}$	$Ag_2(Pb,As)Sb(Sb,As)As_3S_{10}$
Meerschautite	$(Ag,Cu)_{5.5}Pb_{42.4}(Sb,As)_{45.1}S_{112}O_{0.8}$	$Pb_{2.30}(Sb_{3.00}As_{0.70})_{\Sigma 3.70}S_8O$ + $Cu_{0.50}Ag_2(Sb_{3.15}As_{1.35})_{\Sigma 4.50}S_8$
Hypoth. M1	$Ag_2Pb_{20}(Sb,As)_{24}S_{56}O$	$Pb_2(Sb,As)_4S_8O$
Hypoth. M2	$Cu_{0.5}Ag_3Pb_{22}(Sb,As)_{21.5}S_{56}$	$Cu_{0.5}Ag_2(Sb,As)_{\Sigma 4.5}S_8$
Tubulite ?	$Ag_2Pb_{22}Sb_{20}S_{53}$	?

O site, did not allow such splitting to be resolved accurately.

The $Sb/(Sb+As)_{at.}$ of the X-ray formula, 0.850, agrees with that of formulae (1) and (2), 0.847 and 0.842, respectively.

Relationships with sterryite, parasterryite and tubulite

Meerschautite is an expanded derivative of owyheeite (Table 5); the topological derivation of meerschautite from owyheeite is very similar to the derivations described by Moëlo *et al*. (2012) for sterryite and parasterryite. Whereas in these two latter minerals, only one kind of short arm occurs (different between sterryite and parasterryite), two kinds of short arms are present in meerschautite, as described above. According to Makovicky (1997), the derivation of meerschautite from owyheeite can be considered a case of plesiotypism. In agreement with Moëlo *et al*. (2012), the fact that the structures of meerschautite, sterryite and parasterryite can be derived from a common structure (owyheeite) adding two very close types of ribbons (i.e. short and long arms) allows these phases to be considered as a limit case of homeotypy, acting principally by a complex chemical substitution on the short arm(s) of the complex columns.

Meerschautite seems also to be related to the recently described mineral tubulite, $\sim Ag_2Pb_{22}Sb_{20}S_{53}$ (Moëlo *et al*., 2013). Like tubulite, the monoclinic symmetry of meerschautite is related to the β angle between the short (~8 Å) and medium (~27 Å) axes, while in sterryite and parasterryite the β angle is between the short (~8 Å) and the long (~43 Å) axes. Unfortunately, the crystal structure of tubulite is unknown, owing to the peculiar cylindrical shape of the crystals studied. It probably shows two types of chemical connections between complex columns like in meerschautite, but there are some significant differences between these two compounds. Indeed, despite significant As substituting for Sb, meerschautite has a cell volume ~4% higher than tubulite. In meerschautite, the *b*/*c* ratio is 1.537, to be compared with 1.573 in tubulite. For comparison, in sterryite and parasterryite the *c*/*b* ratios are 1.507 and 1.570, respectively. In this group of complex lead-antimony-arsenic sulfosalts, such small differences are indicative of structural changes. Silver is an essential component, occupying specific atom positions, mainly located in the column connections. In the unit formulae (with $Z = 4$), there are four Ag positions in parasterryite, three in sterryite, 2.5 in meerschautite, and probably only two in tubulite.

The formation of such a variety of complex structures by minor chemical changes, essentially

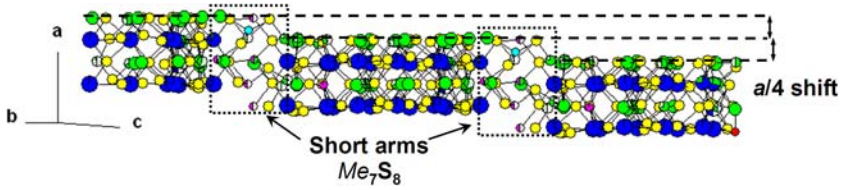

FIG. 10. The **a**/4 shift on the Ag-rich short arm of the column layer of meerschautite. Long arms have been omitted, for clarity.

TABLE 7. Lead-antimony oxy-sulfosalts.

	Chemical formula	$(O:S)_{at.}$ ratio	Sb–O (Å)	(Pb/Sb)–O (Å)	Sb–O–Sb (°)
Chovanite[1*]	$Pb_{15-2x}Sb_{14+2x}S_{36}O_x$ ($x \sim 0.2$)	0.005	2.18 x 2	2.98	141
Chovanite Pollone[2]	$Pb_{13.8}(Sb,As)_{15.2}S_{36}O_{0.6}$	0.017	1.93, 1.95	2.96	139
Pellouxite[3*]	$(Cu,Ag)_2Pb_{21}Sb_{23}S_{55}ClO$	0.018	2.01 x 2	2.81	129
Pillaite[4*]	$Pb_9Sb_{10}S_{23}ClO_{0.5}$	0.022	2.21 x 2	2.81	138
Rouxelite[5*]	$Cu_2HgPb_{22}Sb_{28}S_{64}(O,S)_2$	0.031	2.05 x 2		163
Scainiite[6]	$Pb_{14}Sb_{30}S_{54}O_5$	0.093	1.98 x 2	2.80	131
Meerschautite[7]	$(Ag,Cu)_{5.5}Pb_{42.4}Sb_{45.1}S_{112}O_{0.8}$	0.007	1.84, 2.14	2.82	148

[1]Topa *et al*. (2012); [2]unpublished data; [3]Palvadeau *et al*. (2004); [4]Meerschaut *et al*. (2001); [5]Orlandi *et al*. (2005); [6]Moëlo *et al*. (2000); [7]this work. The symbol * indicates averaged 4 Å structure.

acting on the nature of the short arm connecting fundamental columns, is remarkable. More strange is the formation of meerschautite, which combines two chemically very different short arms, when it seems possible to envisage two simplest, primitive compounds, formed by one or the other of these two arms, with formulas directly derived from those of columns A and B, i.e. $Ag_2Pb_{20}(Sb,As)_{24}S_{56}O$ (M1) and $Cu_{0.5}Ag_3Pb_{22}(Sb,As)_{21.5}S_{56}$ (M2), respectively (Table 6). Projection along **b** of one column layer (without the short arms) shows (Fig. 10) that the monoclinicity of the structure of meerschautite is controlled by an **a**/4 shift on the Ag-rich short arm, while there is no shift at the level of the O-bearing short arm. As a consequence, hypothetical M1 would be a 'shift' structure, like parasterryite, and M2 an 'unshift' one, like sterryite (Moëlo *et al*., 2012).

Meerschautite in the framework of lead-antimony oxysulfosalts and conditions of formation

Meerschautite is the lead-antimony oxysulfosalt with the largest unit formula (over 200 atom positions) with only one specific oxygen position; in addition, together with chovanite, it has the lowest O:S ratio described so far (Table 7). The oxygen position in meerschautite shows quite the same atomic environment as the O3 isolated oxygen position in scainiite (alternating with a vacancy), as well as in pillaite, pellouxite and chovanite. Oxygen is in triangular coordination, with two short Sb–O bonds and one longer Pb–O [or mixed (Pb/Sb)–O in pillaite] bond; only in rouxelite does oxygen have a two-fold coordination, being bonded to two Sb atoms only. Table 7 gives Sb–O distances and Sb–O–Sb angles for similar configurations occurring in these minerals; data from the 8 Å structure of chovanite from a new occurrence from the Pollone mine have been given.

The crystallization of meerschautite, as well as that of chovanite, implies very specific geochemical conditions, with f_{O_2}/f_{S_2} relatively stable. Whereas at Buca della Vena, where several oxysulfosalts have been described, these conditions were apparently assumed by the buffer effect of the iron ore, with the equilibrium between pyrite, hematite and magnetite (e.g. Orlandi *et al*., 1999), at the Pollone mine the same effect could be played by the coexistence of baryte and pyrite. The role of temperature is not known; Costagliola *et al*. (1998) proposed fluid temperature up to 450°C and consequently a temperature >300°C (as for oxysulfosalts from Buca della Vena) can be hypothesized.

The geochemical complexity of the natural hydrothermal solutions is probably the main factor which favours the crystallization of compounds characteristic of multi-component systems; in particular, minor elements (O, Ag and Cu) fill specific atom positions permitting the stabilization of very complex and unpredictable crystal structures like that of meerschautite. The Apuan Alps ore district confirms its role as an extraordinary natural laboratory for the crystallization of very complex sulfosalts, illustrating such processes of increasing structural complexity.

Acknowledgements

Electron-microprobe analyses were performed with the help of J. Langlade (CNRS engineer, "Microsonde Ouest" laboratory, IFREMER, Plouzané, France). Michel Evain is thanked for the useful comments about the crystal structure of meerschautite. The

comments by Peter Leverett and an anonymous reviewer have been greatly appreciated.

References

Aurivillius, B. (1983) The crystal structure of two forms of $BaBi_2S_4$. *Acta Chemica Scandinavica*, **A37**, 399–407.

Biagioni, C., Orlandi, P., Moëlo, Y. and Bindi, L. (2014) Lead-antimony sulfosalts from Tuscany (Italy). XVI. Carducciite, $(AgSb)Pb_6(As,Sb)_8S_{20}$, a new Sb-rich derivative of rathite from the Pollone mine, Valdicastello Carducci: occurrence and crystal structure. *Mineralogical Magazine*, **78**, 1775–1793.

Biagioni, C., Moëlo, Y., Orlandi, P., Stanley, C.J. and Evain, M. (2013) Meerschautite, IMA 2013–061. CNMNC Newsletter No. 17, October 2013, page 3004; *Mineralogical Magazine*, **77**, 2997–3005.

Bindi, L., Keutsch, F.N., Francis, C.A. and Menchetti, S. (2009) Fettelite, $[Ag_6As_2S_7][Ag_{10}HgAs_2S_8]$ from Chañarcillo, Chile: Crystal structure, pseudosymmetry, twinning, and revised chemical formula. *American Mineralogist*, **94**, 609–615.

Brese, N.E. and O'Keeffe, M. (1991) Bond-valence parameters for solids. *Acta Crystallographica*, **B47**, 192–197.

Bruker AXS Inc. (2004) *APEX 2.* Bruker Advanced X-ray Solutions, Madison, Wisconsin, USA.

Costagliola, P., Benvenuti, M., Lattanzi, P. and Tanelli, G. (1998) Metamorphogenic barite-pyrite (Pb-Zn-Ag) veins at Pollone, Apuane Alps, Tuscany: vein geometry, geothermobarometry, fluid inclusions and geochemistry. *Mineralogy and Petrology*, **62**, 29–60.

Guastoni, A., Bindi, L. and Nestola, F. (2012) Debattistiite, $Ag_9Hg_{0.5}As_6S_{12}Te_2$, a new Te-bearing sulfosalt from Lengenbach quarry, Binn valley, Switzerland: description and crystal structure. *Mineralogical Magazine*, **76**, 743–750.

Ilinca, G., Makovicky, E., Topa, D. and Zagler, G. (2012) Cuproneyite, $Cu_7Pb_{27}Bi_{25}S_{68}$, a new mineral species from Băiţa Bihor, Romania. *The Canadian Mineralogist*, **50**, 353–370.

Jambor, J.L. (1967) New lead sulfantimonides from Madoc, Ontario – Part 1. *The Canadian Mineralogist*, **9**, 7–24.

Kerndt, T. (1845) Über die Krystallform und die chemische Zusammensetzung des Geo-Kronits von Val di Castello. *Annalen der Physik*, **141**, 302–307.

Kraus, W. and Nolze, G. (1996) Powder Cell – a program for the representation and manipulation of crystal structures and calculation of the resulting X-ray powder patterns. *Journal of Applied Crystallography*, **29**, 301–303.

Laufek, F., Pažout, R. and Makovicky, E. (2007) Crystal structure of owyheeite, $Ag_{1.5}Pb_{4.43}Sb_{6.07}S_{14}$: refinement from powder synchrotron X-ray diffraction. *European Journal of Mineralogy*, **19**, 557–566.

Léone, P., Le Leuch, L.-M., Palvadeau, P., Molinié, P. and Moëlo, Y. (2003) Single crystal structures and magnetic properties of two iron or manganese-lead-antimony sulfides: $MPb_4Sb_6S_{14}$ (M: Fe, Mn). *Solid State Sciences*, **5**, 771–776.

Makovicky, E. (1985) Cyclically twinned sulphosalt structures and their approximate analogues. *Zeitschrift für Kristallographie*, **173**, 1–23.

Makovicky, E. (1993) Rod-based sulphosalt structures derived from the SnS and PbS archetypes. *European Journal of Mineralogy*, **5**, 54–591.

Makovicky, E. (1997) Modular crystal chemistry of sulphosalts and other complex sulphides. Pp. 237–271 in: *Modular Aspects of Minerals* (S. Merlino, editor). European Mineralogical Union, Notes in Mineralogy, **1**. Eötvös University Press, Budapest.

Meerschaut, A., Palvadeau, P., Moëlo, Y. and Orlandi, P. (2001) Lead-antimony sulfosalts from Tuscany (Italy). IV. Crystal structure of pillaite, $Pb_9Sb_{10}S_{23}ClO_{0.5}$, an expanded monoclinic derivative of hexagonal Bi $(Bi_2S_3)_9I_3$, from the zinkenite group. *European Journal of Mineralogy*, **13**, 779–790.

Meisser, N., Schenk, K., Berlepsch, P., Brugger, J., Bonin, M., Criddle, A.J., Thélin, P. and Bussy, F. (2007) Pizgrischite, $(Cu,Fe)Cu_{14}PbBi_{17}S_{35}$, a new sulfosalt from the Swiss Alps: description, crystal structure and occurrence. *The Canadian Mineralogist*, **45**, 1229–1245.

Mills, S.J., Christy, A.G., Chen, E.C.-C. and Raudsepp, M. (2009) Revised values of the bond valence parameters for $^{[6]}Sb(V)$–O and $^{[3–11]}Sb(III)$–O. *Zeitschrift für Kristallographie*, **224**, 423–431.

Moëlo, Y., Meerschaut, A., Orlandi, P. and Palvadeau, P. (2000) Lead-antimony sulfosalts from Tuscany (Italy): II – Crystal structure of scainiite, $Pb_{14}Sb_{30}S_{54}O_5$, an expanded monoclinic derivative of $Ba_{12}Bi_{24}S_{48}$ hexagonal sub-type (zinkenite group). *European Journal of Mineralogy*, **12**, 835–846.

Moëlo, Y., Orlandi, P., Guillot-Deudon, C., Biagioni, C., Paar, W. and Evain, M. (2011) Lead-antimony sulfosalts from Tuscany (Italy). XI. The new mineral species parasterryite, $Ag_4Pb_{20}(Sb_{14.5}As_{9.5})_{\Sigma 24}S_{58}$, and associated sterryite, $Cu(Ag,Cu)_3Pb_{19}(Sb,As)_{\Sigma 22}(As–As)S_{56}$, from the Pollone mine, Tuscany, Italy. *The Canadian Mineralogist*, **49**, 623–638.

Moëlo, Y., Guillot-Deudon, C. Evain, M., Orlandi, P. and Biagioni, C. (2012) Comparative modular analysis of two complex sulfosalt structures: sterryite, $Cu(Ag,Cu)_3Pb_{19}(Sb,As)_{22}(As\text{-}As)S_{56}$, and parasterryite, $Ag_4Pb_{20}(Sb,As)_{24}S_{58}$. *Acta Crystallographica*, **B68**, 480–492.

Moëlo, Y., Pecorini, R., Ciriotti, M.E., Meisser, N., Caldes, M.T., Orlandi, P., Petit, P.-E., Martini, B. and Salvetti, A. (2013) Tubulite, $\sim Ag_2Pb_{22}Sb_{20}S_{53}$, a new Pb-Ag-Sb sulfosalt from Le Rivet quarry, Peyrebrune ore field (Tarn, France) and Biò, Borgofranco mines,

Borgofranco d'Ivrea (Piedmont, Italy). *European Journal of Mineralogy*, **25**, 1017–1030.

Orlandi, P., Moëlo, Y., Meerschaut, A. and Palvadeau, P. (1999) Lead-antimony sulfosalts from Tuscany (Italy). I. Scainiite, $Pb_{14}Sb_{30}S_{54}O_5$, the first Pb-Sb oxy-sulfosalt, from Buca della Vena mine. *European Journal of Mineralogy*, **11**, 949–954.

Orlandi, P., Moëlo, Y., Meerschaut, A. and Palvadeau, P. (2001) Lead-antimony sulfosalts from Tuscany (Italy). III. Pillaite, $Pb_9Sb_{10}S_{23}ClO_{0.5}$, a new Pb-Sb oxy-chloro-sulfosalt, from Buca della Vena mine. *European Journal of Mineralogy*, **13**, 605–610.

Orlandi, P., Moëlo, Y., Meerschaut, A., Palvadeau, P. and Léone, P. (2004) Lead-antimony sulfosalts from Tuscany (Italy). VI. Pellouxite, ~ $(Cu,Ag)_2Pb_{21}Sb_{23}S_{55}ClO$, a new oxy-chloro-sulfosalt, from Buca della Vena mine, Apuan Alps. *European Journal of Mineralogy*, **16**, 839–844.

Orlandi, P., Meerschaut, A., Moëlo, Y., Palvadeau, P. and Léone, P. (2005) Lead–antimony sulfosalts from Tuscany (Italy). VIII. Rouxelite, $Cu_2HgPb_{22}Sb_{28}S_{64}(O,S)_2$, a new sulfosalt from Buca della Vena mine, Apuan Alps: definition and crystal structure. *The Canadian Mineralogist*, **43**, 919–933

Orlandi, P., Moëlo, Y., Campostrini, I. and Meerschaut, A. (2007) Lead-antimony sulfosalts from Tuscany (Italy). IX. Marrucciite, $Hg_3Pb_{16}Sb_{18}S_{46}$, a new sulfosalt from Buca della Vena mine, Apuan Alps: Definition and crystal structure. *European Journal of Mineralogy*, **19**, 267–279.

Palvadeau, P., Meerschaut, A., Orlandi, P. and Moëlo, Y. (2004) Lead-antimony sulfosalts from Tuscany (Italy). VII. Crystal structure of pellouxite, ~ $(Cu,Ag)_2Pb_{21}Sb_{23}S_{55}ClO$, an expanded monoclinic derivative of $Ba_{12}Bi_{24}S_{48}$ hexagonal sub-type (zinkenite group). *European Journal of Mineralogy*, **16**, 845–855.

Pandeli, E., Bagnoli, P. and Negri, M. (2004) The Fornovolasco schists of the Apuan Alps (Northern Tuscany, Italy): a new hypothesis for their stratigraphic setting. *Bollettino della Società Geologica Italiana*, **123**, 53–66.

Petruk, W., Cabri, L.J., Harris, D.C., Stewart, J.M. and Clark, L.A. (1970) Allargentum, redefined. *The Canadian Mineralogist*, **10**, 163–172.

Pinto, D., Bonaccorsi, E., Balić-Žunić, T. and Makovicky, E. (2008) The crystal structure of vurroite, $Pb_{20}Sn_2(Bi,As)_{22}S_{54}Cl_6$: OD-character, polytypism, twinning and modular description. *American Mineralogist*, **93**, 713–727.

Sheldrick, G.M. (2008) A short history of SHELX. *Acta Crystallographica*, **A64**, 112–122.

Suh, I.-K., Ohta, H. and Waseda, Y. (1988) High-temperature thermal expansion of six metallic elements measured by dilatation method and X-ray diffraction. *Journal of Material Science*, **23**, 757–760.

Topa, D. and Makovicky, E. (2006) The crystal structure of paděraite, $Cu_7(X_{0.33}Pb_{1.33}Bi_{11.33})_{\Sigma 13}S_{22}$, with X = Cu or Ag: new data and interpretation. *The Canadian Mineralogist*, **44**, 481–495.

Topa, D. and Makovicky, E. (2012) Eclarite: new data and interpretations. *The Canadian Mineralogist*, **50**, 371–386.

Topa, D., Sejkora, J., Makovicky, E., Pršek, J., Ozdín, D., Putz, H., Dittrich, H. and Karup-Møller, S. (2012) Chovanite, $Pb_{15-2x}Sb_{14+2x}S_{36}O_x$ ($x \sim 0.2$), a new sulphosalt species from the Low Tatra Mountains, Western Carpathians, Slovakia. *European Journal of Mineralogy*, **24**, 727–740.

Wilson, A.J.C. (1992) *International Tables for Crystallography Volume C.* Kluwer, Dordrecht, The Netherlands.

Zelenski, M., Garavelli, A., Pinto, D., Vurro, F., Moëlo, Y., Bindi, L., Makovicky, E. and Bonaccorsi, E. (2009) Tazieffite, $Pb_{20}Cd_2(As,Bi)_{22}S_{50}Cl_{10}$, a new chloro-sulfosalt from Mutnovsky volcano, Kamchatka Peninsula, Russian Federation. *American Mineralogist*, **94**, 1312–1324.